Mathematical Medicine and Biology (2007) **24**, 251–270
doi:10.1093/imammb/dqm002
Advance Access publication on March 22, 2007

Modelling HA protein-mediated interaction between an influenza virus and a healthy cell: pre-fusion membrane deformation

NAVEEN K. VAIDYA† AND HUAXIONG HUANG‡
Department of Mathematics and Statistics, York University, Toronto, Canada M3J 1P3

AND

SHU TAKAGI§
Department of Mechanical Engineering, The University of Tokyo, Tokyo, Japan

[Received on 29 August 2006; revised on 23 January 2007; accepted on 15 February 2007]

We present a mathematical model for pre-fusion interaction between an influenza virus and a healthy cell. Our model describes the role played by hemagglutinin (HA) protein clusters in bringing the viral membrane into close contact with the host cell membrane as a first step of the fusion process between the two membranes. The viral membrane is modelled as a lipid bilayer with bending rigidity. Using the calculus of variations, we compute the deformation of the viral membrane under the influence of HA protein clusters. Our numerical results support the hypothesis of dimple formation in the fusion site proposed in the literature. The asymmetric nature of the protein molecules due to various reasons such as tilting is the primary cause for the dimple formation. We discuss the effects of spontaneous curvature, the protein cluster radius, fusion-site size and the bending moment exerted by the protein cluster. We also examine the effects of membrane tension and the presence of a host cell on the dimple shape. Our results support previous experimental observations.

Keywords: bending rigidity; equilibrium membrane shape; Euler–Lagrange equations; HA protein; influenza virus; lipid bilayer; membrane pre-fusion.

1. Introduction

A crucial step for an influenza virus to invade a healthy cell is the fusion of the membranes (merging of lipid bilayers) mediated by hemagglutinin (HA) protein. Despite variations in location, timing and frequency, two lipid bilayers have to be brought into close contact for fusion to occur (Blumenthal *et al.*, 2003; Kozlov & Chernomordik, 1998; Kuzmin *et al.*, 2001; Tamm *et al.*, 2003b; Zimmerberg *et al.*, 1993). On the other hand, when an influenza virus first attaches to a viral receptor containing sialic acid, the viral and target membranes are separated by 13.5 nm (the height of the viral spike protein) (Wiley & Skehel, 1987; Zimmerberg *et al.*, 1993), which is too far apart for fusion to occur. Therefore, understanding the pre-fusion mechanism, i.e. how HA protein brings two membranes close to each other, is important for various purposes such as disease control and drug design.

In modelling the fusion mechanism, most efforts have been put into the study of an intermediate structure called the fusion stalk (a local lipidic connection between the proximal, i.e. contacting, monolayers of the fusing membranes) (Kozlov & Chernomordik, 2002; Kozlovsky *et al.*, 2002; Kozlovsky &

†Email: nvaidya@mathstat.yorku.ca
‡Corresponding author. Email: hhuang@mathstat.yorku.ca
§Email: takagi@mech.t.u-tokyo.ac.jp

Kozlov, 2002; Markin & Albanesi, 2002; May, 2002; Zimmerberg *et al.*, 1993). The main focus is on building models in which the predicted energy in a stalk reaches a physically reasonable level (i.e. the required energy is sufficiently low) while assuming that there exists a source of energy required to form a stalk. In fact, a main source of the energy for stalk formation is the energy accumulated during the pre-fusion process. Therefore, it is important to study the dependence of energy on various parameters such as the bending moments exerted by the protein cluster, protein cluster size and fusion-site size during pre-fusion. This will shed light on the possibility of stalk formation as an intermediate stage of the fusion process and consequently the possibility of a successful fusion event. Study of pre-fusion is also useful for the purpose of drug design as the general idea behind modern antiviral drug design is to identify viral proteins, or parts of proteins, that can be disabled. Despite being an important component of the fusion process, the pre-fusion process has not received much attention until recently (Kozlov & Chernomordik, 1998; Kuzmin *et al.*, 2001).

Kozlov & Chernomordik (1998) hypothesized that the activated HA protein can produce viral membrane dimples surrounded by a ring-like cluster of HA. Assuming that the top of the dimple is a segment of a perfect sphere connected to a funnel of catenoid form (an axisymmetric surface with zero mean curvature), the energy in the dimple was estimated and found to be sufficient to cause instability of the lipid bilayers (Kozlov & Chernomordik, 1998). Similarly, Kuzmin *et al.* (2001) assumed a perfect spherical shape for the top of the dimple (nipple in their terminology). The formation of a dimple was also favoured as a mechanism for membranes to make intimate contact which leads to subsequent fusion between membranes (Markosyan *et al.*, 1999).

In this study, we propose a model for pre-fusion membrane deformation in the form of an energy functional. Our model is a generalization of the one given by Kozlov & Chernomordik (1998), which incorporates the energy contribution due to the bending rigidity of the membrane and the energy due to HA protein. Our main objective is to verify the hypothesis of dimple formation (Kozlov & Chernomordik, 1998; Kuzmin *et al.*, 2001; Markosyan *et al.*, 1999) without assuming a specific shape of the viral membrane. Our numerical results confirm the dimple formation and give a more accurate estimate of the extra energy accumulated inside the dimple area.

Experimental work by Markosyan *et al.* (1999) has revealed that membrane tension inhibits fusion. This suggests that the tension created in the membrane, which was neglected in previous studies (Kozlov & Chernomordik, 1998; Kuzmin *et al.*, 2001), may play a crucial role in the fusion/pre-fusion process. Therefore, we also examine pre-fusion deformation under tension and our result is consistent with experimental observations (Markosyan *et al.*, 1999). Furthermore, when a dimple forms, the presence of the host cell membrane may have an effect on viral membrane deformation. This is also investigated in this paper along with the effects of spontaneous curvature, the fusion-site radius, the protein cluster radius and the applied bending moments. The effect of the spontaneous curvature predicted by our model is in good agreement with the experimental observations (Markosyan *et al.*, 1999).

2. Model

Even though the influenza viral membrane consists of two types of proteins, HA and neuraminidase, it has been suggested that HA is the one which facilitates the fusion of the lipid bilayers (Stegmann, 1993). Therefore, we consider only HA protein in our model. HA is a glycoprotein which consists of a trimer with an individual monomer having HA1 and HA2 subunits (Blumenthal *et al.*, 2003; Gruenke *et al.*, 2002; Kozlov & Chernomordik, 1998; Li *et al.*, 2005; Markovic *et al.*, 2001; Tamm, 2003; Tamm *et al.*, 2003a,b). It is believed that HA1 is responsible for virus attachment to the cell surface via a sialic acid-binding site and HA2 activates the fusion process. During low-pH activation (e.g. when the

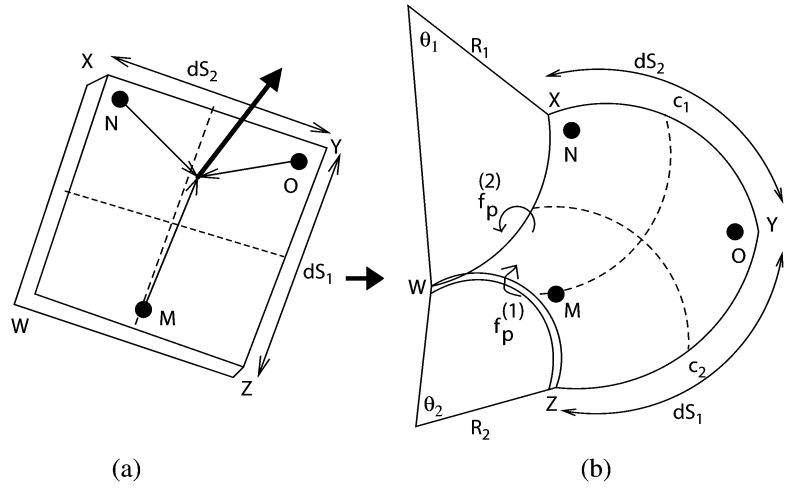

FIG. 1. (a) Undeformed and (b) deformed state of a small membrane section $WXYZ$ containing a HA trimer. M, N and O are the positions of HA monomers anchored to the membrane and the thick arrow indicates a triple-stranded, α-helical coiled coil. c_1 and c_2 are principal curvatures developed in the deformed membrane along the arc length directions $\mathrm{d}S_1$ and $\mathrm{d}S_2$, respectively. R_1 and R_2 are radii of principal curvature. θ_1 and θ_2 are angles subtended by the circular curved membrane at the centre.

protein is exposed to a pH 5 environment), the hydrophobic fusion peptide, previously hidden within the trimeric stem, is projected towards viral and/or target membranes (Blumenthal *et al.*, 2003; Gaudin *et al.*, 1995; Kozlov & Chernomordik, 1998; Skehel & Wiley, 2000). The subsequent refolding of the protein exerts a force on the fusion peptide inserted into the membrane. A similar process takes place in the target membrane due to a protein force (via inserted fusion peptide), but for simplicity we focus only on the viral membrane in this study.

The precise mechanism of how an HA trimer exerts force on a membrane could be quite complex. Kozlov & Chernomordik (1998) proposed that the net effect of these HA trimers can be modelled by a bending moment acting on a saddle-shaped membrane. In this paper, we use a similar but less restrictive model, outlined below.

Following Kozlov & Chernomordik (1998), we consider a small section of the viral membrane containing an embedded HA trimer. Figure 1(a) shows a section $WXYZ$ of undeformed (neutral pH) rectangular membrane with sides $YZ = \mathrm{d}S_1$, $XY = \mathrm{d}S_2$ and area $\mathrm{d}A = \mathrm{d}S_1\,\mathrm{d}S_2$. M, N and O are positions of three monomers anchored in the membrane, connected to each other forming a triple-stranded, α-helical coiled coil. When the pH value is lowered, recruitment of additional residues to the coiled coil takes place (Bullough *et al.*, 1994; Carr & Kim, 1993; Kozlov & Chernomordik, 1998). This results in an increase of the coiled-coil rigid rod in some direction, e.g. the direction indicated by the arrow in the middle. The coiled coil exerts forces on the membrane at anchor positions, shown by the arrows originated from M, N and O. Since a HA trimer can be tilted from the normal direction of the membrane (Bentz, 2000; Tamm, 2003; Tatulian *et al.*, 1995), the forces acting at M, N and O are asymmetric. As a result of forces due to coiled coil and HA molecule tilting, the membrane deforms, cf. Fig. 1(b).

Let c_1 and c_2 be the two principal curvatures of the deformed membrane, cf. Fig. 1(b). We assume that the four sides of the segment $WXYZ$ coincide with the principal directions with lengths $\mathrm{d}S_1$ and $\mathrm{d}S_2$ along the directions of c_1 and c_2, respectively. Since our focus in this paper is to analyse the

axisymmetric shape of the membrane, we also assume that the principal directions of the bending moment tensor are same as those of the curvature tensor. Let $f_{\mathrm{p}}^{(1)}$ be the bending moment per unit length exerted by HA protein along the two edges XY and WZ. To produce a curvature c_1, the work performed by the bending moment per unit length in the S_2 direction is $f_{\mathrm{p}}^{(1)}\theta_1/2$, where θ_1 is the angle subtended by the circular curved membrane at the centre of the circle and R_1 is the corresponding radius (Gere, 2004; Hibbeler, 2005). Note that $\theta_1 = \mathrm{d}S_1/R_1 = c_1\,\mathrm{d}S_1$; therefore, the work performed to produce a curvature c_1 in the membrane segment is $\mathrm{d}\omega_1 = f_{\mathrm{p}}^{(1)}c_1\,\mathrm{d}S_1\,\mathrm{d}S_2/2 = f_{\mathrm{p}}^{(1)}c_1\,\mathrm{d}A/2$. Similarly, if $f_{\mathrm{p}}^{(2)}$ is the bending moment per unit length, exerted by a HA protein along the two edges WX and YZ, the work performed to produce a curvature c_2 in the membrane segment is $\mathrm{d}\omega_2 = f_{\mathrm{p}}^{(2)}c_2\,\mathrm{d}S_1\,\mathrm{d}S_2/2 = f_{\mathrm{p}}^{(2)}c_2\,\mathrm{d}A/2$. Therefore, the total work performed by the protein in bending the membrane element $WXYZ$ is $\mathrm{d}\omega = \mathrm{d}\omega_1 + \mathrm{d}\omega_2 = (f_{\mathrm{p}}^{(1)}c_1 + f_{\mathrm{p}}^{(2)}c_2)\mathrm{d}A/2$.

Kozlov & Chernomordik (1998) assumed that the two principal curvatures are equal in value with opposite signs, i.e. $c_1 = -c_2 = c_{\mathrm{p}}$. The total contribution of a HA trimer to the membrane energy is given by integrating $\tau_{\mathrm{p}}c_{\mathrm{p}}$ over the cluster area, where τ_{p} is a bending moment applied by the protein to the unit length of the circumference of the membrane fragment. In this paper, we relaxed the assumption made by Kozlov & Chernomordik (1998) without imposing $c_1 = -c_2 = c_{\mathrm{p}}$ (a perfect saddle shape) *a priori*. Instead, we note that force due to refolding takes place in a certain direction depending upon the tilting of HA molecule and tilting has been observed in experiments (Bentz, 2000; Tamm, 2003; Tatulian *et al.*, 1995). As a consequence of this asymmetry of the forces (due to refolding of protein including tilting) acting at anchor positions, the resulting bending moments $f_{\mathrm{p}}^{(1)}$ and $f_{\mathrm{p}}^{(2)}$ in general take different values. For example, they could have the same sign but different magnitudes.

We assume that the viral membrane can resist bending and the shape of the membrane is determined by minimizing a Helfrich-type energy functional in addition to the energy induced by the bending moments. The energy functional takes the form

$$E = \frac{1}{2}k_{\mathrm{b}}\int (c_1 + c_2 - c_0)^2\,\mathrm{d}A + k_{\mathrm{g}}\int c_1c_2\,\mathrm{d}A + \frac{1}{2}\int (f_{\mathrm{p}}^{(1)}c_1 + f_{\mathrm{p}}^{(2)}c_2)\mathrm{d}A. \tag{2.1}$$

Here, the first two terms are the Helfrich (1973) energy due to the bending rigidity and the Gaussian bending rigidity of the membrane, respectively. The last term is an energy contribution due to the work done by the HA protein. k_{b} and k_{g} are the bending rigidity and the Gaussian bending rigidity, respectively, and c_0 denotes the spontaneous curvature, which takes the possible asymmetry of the bilayer into account. When $k_{\mathrm{g}} = 0$, $c_0 = 0$, $c_1 = -c_2 = c_{\mathrm{p}}$ and $f_{\mathrm{p}}^{(1)} = -f_{\mathrm{p}}^{(2)} = -\tau_{\mathrm{p}}$, our model reproduces the saddle-shaped membrane fragment proposed by Kozlov & Chernomordik (1998).

As shown by experimental observations (Markosyan *et al.*, 1999), tension developed in the membranes inhibits fusion. This suggests that the tension created in the lipid bilayer membrane may have considerable impact on the pre-fusion process. We model the membrane under the tension by adding a term into the model as follows (Boal, 2002):

$$E = \frac{1}{2}k_{\mathrm{b}}\int (c_1 + c_2 - c_0)^2\,\mathrm{d}A + k_{\mathrm{g}}\int c_1c_2\,\mathrm{d}A + \frac{1}{2}\int (f_{\mathrm{p}}^{(1)}c_1 + f_{\mathrm{p}}^{(2)}c_2)\mathrm{d}A + \gamma\int \mathrm{d}A, \tag{2.2}$$

where γ is an in-plane tension (tensile stress) developing in the membrane. In this study, the value of γ will be varied to examine the effect of membrane tension.

In the following sections, we discuss how to compute the pre-fusion deformation of the viral membrane based on the energy functional given by (2.1) and (2.2).

3. Shape equations of an axisymmetric viral membrane

For the rest of the paper, we focus exclusively on an axisymmetric membrane. In this section, the axisymmetric shape equations of the membrane related to the energy functionals (2.1) and (2.2) are given, followed by the shape equation for a viral membrane constrained by the presence of a cell membrane.

3.1 *Shape equation related to energy functional (2.1)*

The equilibrium membrane shape can be obtained by minimizing the energy functional (2.1) directly. In this paper, we use an indirect method by deriving an Euler–Lagrange equation (so-called shape equation in the physics literature). Since our objective is to model and analyse the membrane behaviour during the pre-fusion state without the merging of the viral and the host cell membranes, the viral membrane does not experience a topological change. This allows us to drop the Gaussian curvature term in (2.1). Considering an axisymmetric viral membrane, illustrated in Fig. 2, and using the expression for curvatures

$$c_1 = \cos\psi \frac{\mathrm{d}\psi}{\mathrm{d}\rho}, \quad c_2 = \frac{\sin\psi}{\rho}, \tag{3.1}$$

the energy functional (2.1) can be written as

$$E_1 = \pi \int_0^{\rho_f} \mathcal{L}\, \mathrm{d}\rho, \tag{3.2a}$$

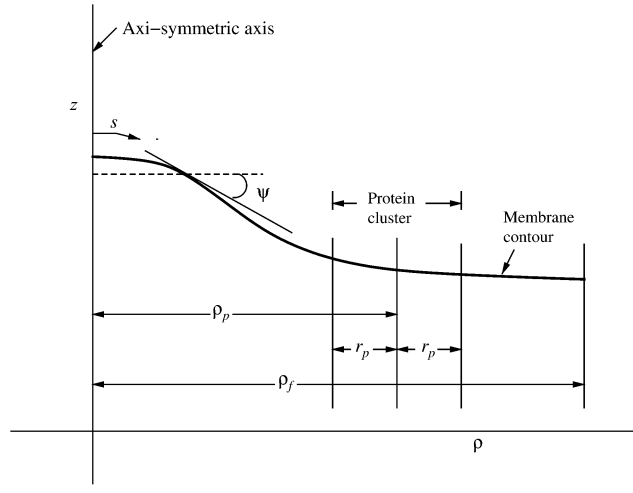

FIG. 2. Schematic diagram of the axisymmetric viral membrane with the z-axis as the axis of symmetry. s is the arc length, ρ is the distance to the symmetric axis, ψ is the angle made by the tangent to the membrane with the plane perpendicular to the axis of symmetry, ρ_f is the maximum distance of the membrane considered, ρ_p is average of the internal and external radii of the protein ring and r_p is half of the width (size) of the protein ring.

where

$$\mathcal{L} = k_b \rho \cos\psi \left(\frac{d\psi}{d\rho}\right)^2 + 2k_b \sin\psi \frac{d\psi}{d\rho} + \frac{k_b \sin^2\psi}{\rho\cos\psi} + f_p^{(1)} \rho \frac{d\psi}{d\rho} + \frac{f_p^{(2)} \sin\psi}{\cos\psi}$$
$$+ \frac{k_b \rho c_0^2}{\cos\psi} - 2c_0 k_b \rho \frac{d\psi}{d\rho} - \frac{2k_b c_0 \sin\psi}{\cos\psi} + \eta\left(\cos\psi \frac{dz}{d\rho} + \sin\psi\right) \tag{3.2b}$$

and ρ_f is the maximum distance of the membrane considered from the axis of symmetry. Here, we have incorporated the geometric constraint $\cos\psi\, dz + \sin\psi\, d\rho = 0$ via a Lagrangian multiplier η.

Using the calculus of variations, the energy functional (3.2a) provides us with the following Euler–Lagrange equations (see Appendix A):

$$\mathcal{H} = 0, \tag{3.3a}$$

$$\cos\psi \frac{dz}{d\rho} = -\sin\psi, \tag{3.3b}$$

$$\eta\cos\psi = \eta_0, \tag{3.3c}$$

where η_0 is an integration constant and

$$\mathcal{H} = \cos^2\psi \frac{d^2\psi}{d\rho^2} - \frac{\sin 2\psi}{4}\left(\frac{d\psi}{d\rho}\right)^2 - \frac{\sin 2\psi}{4\rho^2} - \frac{\sin\psi}{2\rho^2\cos\psi} + \frac{\cos^2\psi}{\rho}\frac{d\psi}{d\rho} + \frac{f_p^{(1)}\cos\psi}{2k_b\rho}$$
$$+ \frac{\cos\psi}{2k_b}\frac{d f_p^{(1)}}{d\rho} - \frac{f_p^{(2)}}{2k_b\rho\cos\psi} - \frac{\eta}{2k_b\rho} - \frac{c_0^2\sin\psi}{2\cos\psi} + \frac{c_0\sin^2\psi}{\rho\cos\psi}.$$

3.2 *Shape equations related to energy functional (2.2)*

Imposing the axisymmetric condition, the energy functional (2.2) can be rewritten as

$$E_2 = \pi \int_0^{\rho_f} [\mathcal{L} + 2\gamma\rho\sec\psi] d\rho, \tag{3.4}$$

where $\mathcal{L}$ is given by (3.2b). A similar procedure leads the following Euler–Lagrange equations:

$$\mathcal{H} = \frac{\gamma\sin\psi}{k_b\cos\psi}, \tag{3.5a}$$

$$\cos\psi \frac{dz}{d\rho} = -\sin\psi, \tag{3.5b}$$

$$\eta\cos\psi = \eta_0. \tag{3.5c}$$

Here, γ is a prescribed (constant) tension in the membrane.

3.3 *Bending moments induced by HA trimers*

For fusion to occur during conformational change at low pH values, interaction between adjacent HA trimers with high local density results in multiple trimers assembling around the fusion site

(Markovic *et al.*, 2001). These assembled HA trimers can be assumed to form ring-like clusters surrounding the fusion site (Bentz *et al.*, 1990; Blumenthal *et al.*, 1995; Danieli *et al.*, 1996; Kozlov & Chernomordik, 1998; Zimmerberg *et al.*, 1993), and these proteins perform concerted activation to synchronously release the conformational energy (Markovic *et al.*, 2001). Moreover, fusion peptide interaction among neighbouring HAs has been hypothesized to be responsible for a measurable decrease in the lateral mobility of HA after activation (Gutman *et al.*, 1993; Markovic *et al.*, 2001). Based on these observations, we assume that HA trimers are axisymmetrically distributed on a ring formed about the axis of symmetry of the membrane. As a simple model, we also assume that the bending moments $f_{\mathrm{p}}^{(1)}$ and $f_{\mathrm{p}}^{(2)}$ exerted by the protein are given by

$$f_{\mathrm{p}}^{(i)}(\rho) = F_{\mathrm{p}}^{(i)} H(\rho), \quad i = 1, 2, \tag{3.6a}$$

where the Heaviside function $H(\rho)$ is

$$H(\rho) = \begin{cases} 1, & \text{if } |\rho - \rho_{\mathrm{p}}| \leqslant r_{\mathrm{p}}, \\ 0, & \text{otherwise.} \end{cases} \tag{3.6b}$$

Here, $F_{\mathrm{p}}^{(i)}, i = 1, 2$, ρ_{p} and r_{p} are the magnitude of the bending moments exerted by HA protein, the average of the internal and external radii of the protein ring and half of the width of the protein ring, respectively (see Fig. 2). The derivative of the Heaviside function is a delta function, and the derivative of $f_{\mathrm{p}}^{(i)}(\rho)$ is given by

$$\frac{\mathrm{d} f_{\mathrm{p}}^{(i)}}{\mathrm{d}\rho} = \operatorname{sign}\left(F_{\mathrm{p}}^{(i)}\right) \begin{cases} 0, & 0 \leqslant \rho < \rho_{\mathrm{p}} - r_{\mathrm{p}}, \\ \infty, & \rho = \rho_{\mathrm{p}} - r_{\mathrm{p}}, \\ 0, & \rho_{\mathrm{p}} - r_{\mathrm{p}} < \rho < \rho_{\mathrm{p}} + r_{\mathrm{p}}, \\ -\infty, & \rho = \rho_{\mathrm{p}} + r_{\mathrm{p}}, \\ 0, & \rho_{\mathrm{p}} + r_{\mathrm{p}} < \rho \leqslant \rho_f. \end{cases} \tag{3.6c}$$

3.4 *Boundary conditions*

To solve the shape equations, we need to impose proper boundary conditions. Let ρ_f be the distance from the axis of symmetry where the membrane remains undisturbed, i.e. the membrane remains flat (horizontal). At the axis of symmetry $\rho = 0$, we use the symmetry condition $\mathrm{d}z/\mathrm{d}\rho = 0$. In addition, $\mathrm{d}z/\mathrm{d}\rho = -\tan\psi$ implies $\psi = 0$ at $\rho = 0$. Since we assume that the membrane is flat at $\rho = \rho_f$, we obtain $\psi(\rho_f) = 0$. Therefore, to solve the shape equations (3.3a)–(3.3c), we use the following set of boundary conditions:

$$\rho = 0: \ \ \psi = 0, \tag{3.7a}$$

$$\rho = \rho_f: \ \ \psi = 0, \quad z = z_f, \quad \frac{\mathrm{d}\psi}{\mathrm{d}\rho} = 0, \tag{3.7b}$$

where z_f is arbitrary. Since we need an extra boundary condition due to presence of the unknown η_0, we have added a no-flux type of boundary condition at $\rho = \rho_f$, where membrane remains flat.

3.5 *Shape equations constrained by the cell membrane*

So far we have ignored possible interactions between the viral and the host cell membranes. As the two membranes are brought into close contact, we need to consider the deformation of both membranes and their effect on each other. To simplify the discussion, we assume that the presence of the host membrane imposes a maximum height for the deformed viral membrane. As a result, we have a contact problem, which can be treated under our general framework by imposing an additional constraint. As a simple model, we incorporate the presence of a target membrane as an opposing surface for the viral membrane via an inequality $z \leqslant z_{\rm h}$, where $z_{\rm h}$ is the maximum height allowed when the viral membrane meets the host cell membrane.

Following Sage (1968), we implement the inequality constraint by changing it into an equality constraint as $z_{\rm h} - z = \xi^2$. Here, ξ represents the square root of the vertical distance between the cell membrane and the viral membrane. We allow ξ to take on only real values so that $z_{\rm h} - z$ will always be positive and satisfy the required constraint $z \leqslant z_{\rm h}$. Again, we apply this equality constraint via a Lagrangian multiplier ζ so that the energy functional for the constrained membrane takes the form of

$$E_3 = \int_0^{\rho_f} [\pi \mathcal{L} + \zeta(z - z_{\rm h} + \xi^2)]{\rm d}\rho, \tag{3.8}$$

where $\mathcal{L}$ is given by (3.2b). The corresponding Euler–Lagrange equations are

$$\mathcal{H} = 0, \tag{3.9a}$$

$$\cos\psi \frac{{\rm d}\eta}{{\rm d}\rho} = \zeta + \eta \sin\psi \frac{{\rm d}\psi}{{\rm d}\rho}, \tag{3.9b}$$

$$\cos\psi \frac{{\rm d}z}{{\rm d}\rho} = -\sin\psi, \tag{3.9c}$$

$$z - z_{\rm h} = -\xi^2, \tag{3.9d}$$

$$\zeta\xi = 0. \tag{3.9e}$$

Algebraic manipulations show that (3.9c) and (3.9d) can be replaced by the following equation:

$$2\xi \cos\psi \frac{{\rm d}\xi}{{\rm d}\rho} = \sin\psi. \tag{3.9f}$$

Equations (3.9a), (3.9b), (3.9e) and (3.9f) can be solved using boundary conditions

$$\psi(0) = 0, \quad \psi(\rho_f) = 0, \quad \eta(0) = 0, \quad \xi(\rho_f) = \sqrt{z_{\rm h} - z_f}. \tag{3.9g}$$

Note that $\eta \cos\psi$ is no longer a constant in this case.

4. Results and discussion

The numerical results are obtained using the solution methodology summarized in Appendix B. Before presenting the results, we note briefly that the value of ρ_f, where the membrane becomes flat, should be sufficiently large. In practice, it depends on the density of the activated HA trimers. As mentioned by Kozlov & Chernomordik (1998), the contact area of a radius ~25 nm can have ~10 dimples if all

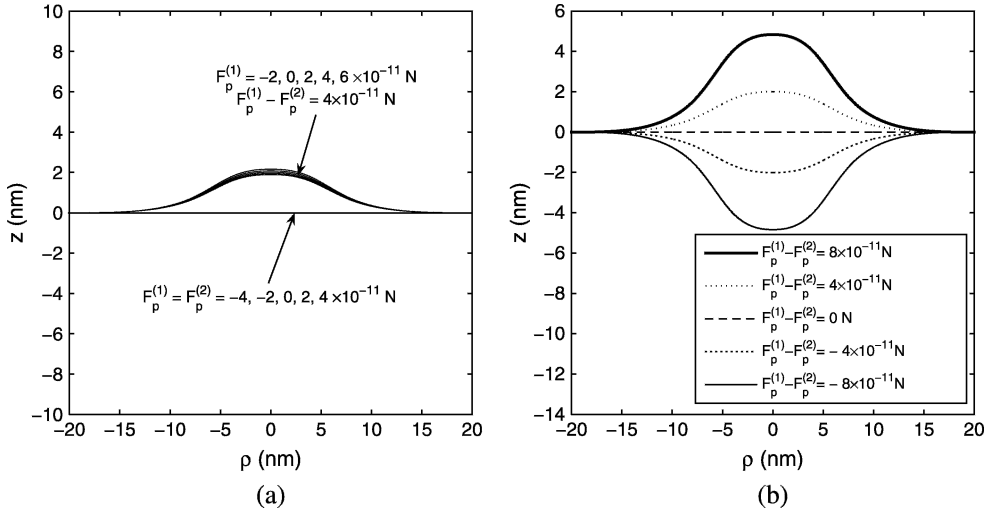

FIG. 3. (a) Shape of the viral membrane for different $F_p^{(1)}$ and $F_p^{(2)}$ but with the same $F_p^{(1)} - F_p^{(2)}$. (b) Shape of the viral membrane for the different values of $F_p^{(1)} - F_p^{(2)}$.

the HA molecules in this area are activated. This allows us to estimate the range of ρ_f to be from 8 to 25 nm and in our computations we set $\rho_f = 20$ nm. For all computations, the bending rigidity is given as $k_b = 20kT$ as in Kozlov & Chernomordik (1998), where k is the Boltzman constant and T is the temperature.

In the following, we first present numerical results obtained by taking a various combinations of the bending moments $F_p^{(1)}$ and $F_p^{(2)}$ (within an appropriate range). Our results show that membrane deformation is related mainly to the difference between the two applied bending moments, $\Delta F_p = F_p^{(1)} - F_p^{(2)}$. In other words, the deformation of the membrane remains almost the same when ΔF_p is fixed, regardless of the values and signs of $F_p^{(1)}$ and $F_p^{(2)}$. Figure 3(a) shows the membrane deformation for two cases, namely, $\Delta F_p = 0$ N, i.e. $F_p^{(1)} = F_p^{(2)}$, and $\Delta F_p = 4 \times 10^{-11}$ N, with the different magnitudes of $F_p^{(1)}$ and $F_p^{(2)}$ (including both negative, both positive and opposite signs). When $\Delta F_p = 0$, the membrane shape remains planar. For the other case, the difference in deformation is small. Moreover, the effect of ΔF_p on the membrane equilibrium shape is shown in Fig. 3(b). Nonzero ΔF_p causes the membrane to deform and the direction depends on the sign of ΔF_p. An increase in the magnitude of ΔF_p increases the dimple height from the planar state.

Recall that in the case of membrane fusion, Kozlov & Chernomordik (1998) assume that the viral membrane deforms into a saddle shape at the protein sites with equal bending moments. Our results show that it is not necessary to make assumptions on the curvature of the deformation and the nature of the bending moments. The most relevant quantity is the difference of the two principal bending moments. Because of the asymmetric nature of the protein force, the difference between the bending moments ΔF_p is usually nonzero, regardless of their signs. Therefore, our model and results are much more general.

Since $F_p^{(1)} - F_p^{(2)}$ is the relevant quantity, instead of the magnitudes of individual $F_p^{(1)}$ and $F_p^{(2)}$, for membrane deformation, we define $F_p^{(1)} - F_p^{(2)} = 2F_p$. We use F_p as the primary variable so that

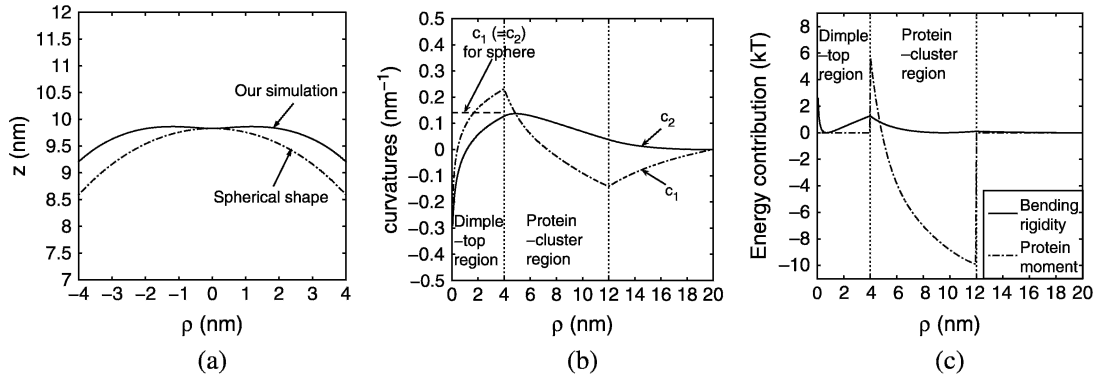

FIG. 4. (a) Dimple top shape produced by our model compared with a sphere. (b) Principal curvatures of the membrane. (c) Energy contribution due to the bending rigidity and bending moments exerted by the protein.

direct comparison can be made with the result in Kozlov & Chernomordik (1998). Moreover, a change in the sign of F_p simply changes the direction of the dimple formation. With the assumption that the host cell lies above the viral membrane, the relevant direction for viral membrane deformation is upwards. Therefore, in the rest of the paper, only the results with $F_p \geqslant 0$ are presented. In addition, we will simply refer to F_p as the bending moments (instead of the difference of the bending moments) from the protein clusters (HA trimers).

4.1 *Deformation of tensionless membranes*

For comparison purposes, we have carried out simulations using a fixed set of parameter values, which are $F_p = 2.4 \times 10^{-11}$ N, $c_0 = 0$, $\rho_p = 8$ nm and $r_p = 4$ nm, which result in a fusion site with a size of $\rho_p - r_p = 4$ nm as in Kozlov & Chernomordik (1998).

Assuming the dimple top is a segment of a sphere with radius 7.0841 nm, it was estimated in Kozlov & Chernomordik (1998) that the angle ψ at the edge of the dimple top is approximately 0.6 rad. In Fig. 4(a), we plot this segment (dot-dashed line) along with the dimple top produced by our model. It can be seen that the spherical approximation gives only a qualitatively consistent shape. This can be seen more clearly in Fig. 4(b), where the two principal curvatures are plotted. For a spherical shape, both curvatures are constant and equal. However, the curvatures produced by our (more general) model are not constant. Moreover, the mean curvature, $0.5(c_1 + c_2)$, does not vanish in the protein cluster region, contrary to the catenoid shape in the protein cluster region hypothesized by Kozlov & Chernomordik (1998).

The distributions of the energy contribution due to bending rigidity and protein bending moments are plotted in Fig. 4(c). Inside the dimple top, the contribution is mainly due to the bending rigidity while in the protein cluster region, the dominating contribution comes from the bending moments exerted by the protein. In order to facilitate fusion, a significant amount of energy must be available for the monolayers to overcome an energy barrier and merge. From our numerical results, we estimate that the energy stored inside the dimple top is approximately 37.43 kT when the height of the dimple top is 9.8 nm. This energy level is in accordance with the energy barrier of ≈37 kT for the merging of monolayers (Kuzmin *et al.*, 2001; Markin & Albanesi, 2002). Since a sufficient amount of energy can be stored inside the dimple top due to the bending moments exerted by the protein cluster, our results support the mechanism proposed by Kozlov & Chernomordik (1998), despite the fact that the dimple shape is far from spherical.

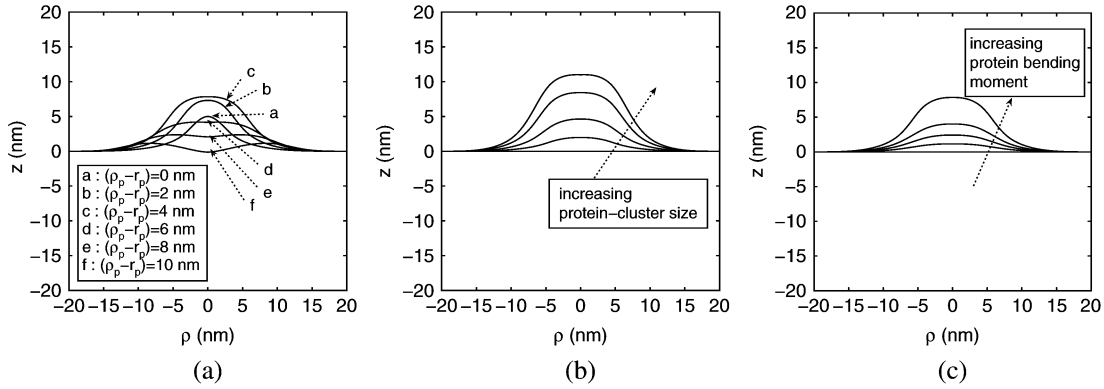

FIG. 5. Equilibrium shape of the viral membrane for (a) different fusion-site radii, (b) different protein cluster sizes and (c) different magnitudes of the bending moment exerted by HA protein.

In Fig. 5(a), we plot the membrane shape as the size of the fusion site $\rho_p - r_p$ is varied. We note that near the axis of symmetry, the curvature could change signs for some values of $\rho_p - r_p$. This further suggests that the assumption of a spherical shape for the dimple top is not valid. Our results also suggest that there might exist an optimal value of $\rho_p - r_p$ for the HA molecules to form clusters. This can be illustrated further by examining the energy stored in the membrane. For $F_p = 2 \times 10^{-11}$ N, $c_0 = 0$ and $r_p = 2$ nm, the energy stored inside the dimple top and the total energy in the membrane as a function of $\rho_p - r_p$ are plotted in Figs 6(b) and 7(b), respectively. Here, the total energy in the membrane is computed by integrating the energy on the entire membrane segment (from $\rho = 0$ to $\rho = \rho_p + r_p$) and the energy stored inside the dimple top is obtained by integrating only to the edge of fusion site (from $\rho = 0$ to $\rho = \rho_p - r_p$). It can be seen from Fig. 7(b) that the energy stored inside the dimple top attains a maximum value at a critical value of $\rho_p - r_p = 2.75$ nm, comparable to the value of r_p. This result is consistent with the discussion in Kozlov & Chernomordik (1998), where they found that the inner radius of the cluster is comparable to the radius of the HA trimer cluster.

Next, we examine the effect of protein cluster size $2r_p$ on membrane deformation. We again set $F_p = 2 \times 10^{-11}$ N, $c_0 = 0$ and $\rho_p - r_p = 4$ nm. As shown in Fig. 5(b), increasing protein cluster size leads to bigger dimple height. Total energy in the membrane (including energy by bending rigidity as well as energy due to bending moments exerted by the protein) increases (in its absolute value) as the protein cluster size increases. Energy inside the dimple top also increases with the protein cluster size. This is shown in Figs 6(c) and 7(c). This result is also consistent with the conclusion in Kozlov & Chernomordik (1998).

In Fig. 5(c), it is shown that dimple height grows when the bending moments exerted by the protein cluster increase. In Figs 6(d) and 7(d), total energy in the membrane and the energy inside the dimple top are plotted as functions of the bending moments exerted by protein for $c_0 = 0$, $r_p = 2$ nm and $\rho_p - r_p = 4$ nm. Again the magnitude of the total energy in the membrane is negative and that inside the dimple top is positive. Absolute values of both energies increase with the bending moments. The results indicate that the membrane responds to the protein bending moments by deforming into a particular shape to avoid excessive energy in the protein cluster region and by storing extra energy inside the dimple top.

The effect of spontaneous curvature c_0 (reflecting membrane asymmetry due to composition) on the energy stored in lipid bilayers is of considerable interest and has been a subject of much experimental

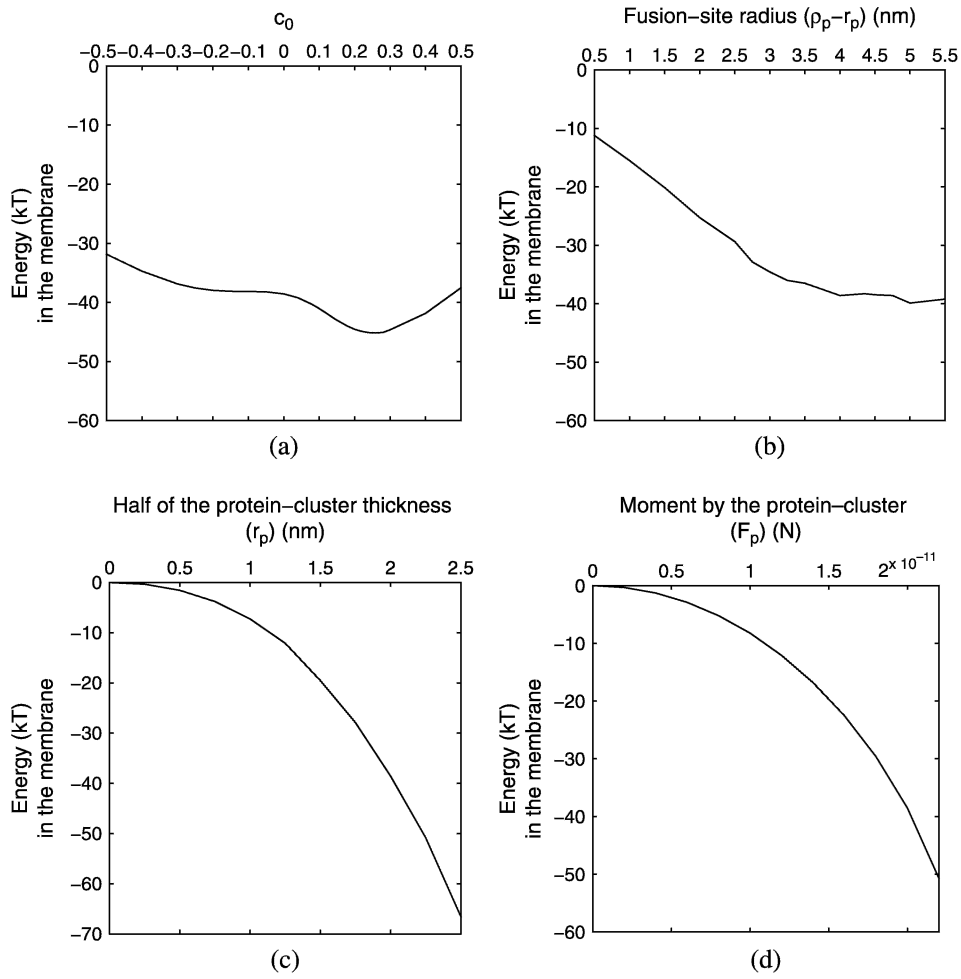

FIG. 6. Energy in the entire membrane (from $\rho = 0$ to $\rho = \rho_p + r_p$) affected by (a) spontaneous curvature c_0, (b) fusion-site radius, (c) protein cluster size and (d) bending moments exerted by HA protein.

work (Markosyan *et al.*, 1999). In Figs 6(a) and 7(a), total membrane energy and the energy inside the dimple top are plotted for $F_p = 2 \times 10^{-11}$ N, $\rho_p = 6$ nm and $r_p = 2$ nm. Both of these energies are not monotonic functions of c_0 and a maximum value of the energy inside the dimple top occurs at a small positive value of c_0. Therefore, our results suggest that a small (positive) spontaneous curvature favours fusion, while a large (positive) spontaneous curvature inhibits fusion. This is consistent with the experimental observation in Markosyan *et al.* (1999), where it was observed that the fusion does not occur in the presence of too many agents with positive spontaneous curvature, such as lysophosphatidylcholine (LPC), but the subsequent removal of LPC leads to fusion.

4.2 *Membranes under tension*

To examine the effect of membrane tension on deformation, we solve (3.5a)–(3.5c). The results are presented in Fig. 8 based on parameter values $F_p = 2.4 \times 10^{-11}$ N, $\rho_p = 6$ nm, $r_p = 2$ nm and

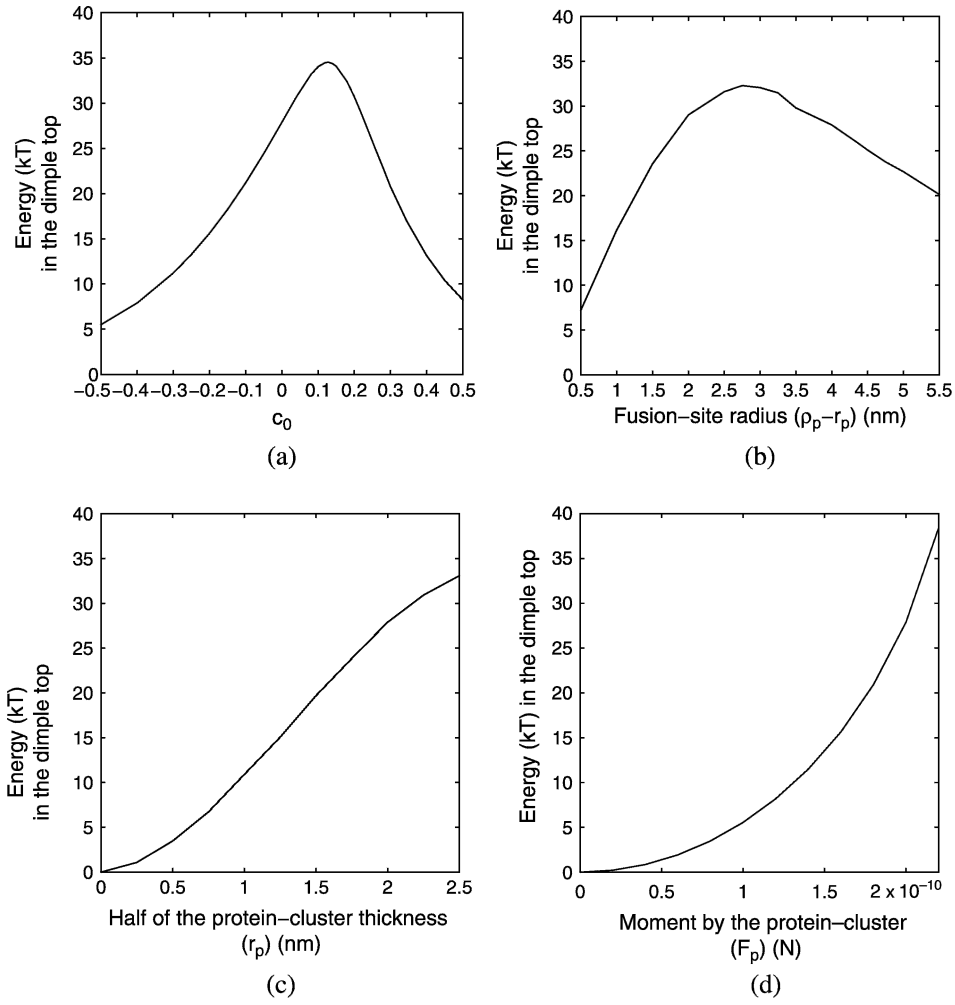

FIG. 7. Energy inside the dimple top (from $\rho = 0$ to $\rho = \rho_p - r_p$) affected by (a) spontaneous curvature c_0, (b) fusion-site radius, (c) protein cluster size and (d) the bending moment exerted by HA protein.

$\gamma = 0, 3, 6, 10 \times 10^{-4}$ N m^{-1}. The plot for $\gamma = 0$ N m^{-1} corresponds to the tension-free membrane discussed earlier. The plots clearly show the effect of the tension γ on dimple height as well as energy stored inside the dimple top. Increasing membrane tension from 0 to 10×10^{-4} N m^{-1} reduces dimple height. The energy stored inside the dimple top also drops from 55.40 to 36.28 kT. Therefore, membrane tension makes it more difficult for the membrane to form a dimple and store energy, thereby inhibiting fusion. Our results strongly support the experimental observation in Markosyan *et al.* (1999), where it was shown that membrane tension prevents dimple formation and inhibits fusion.

4.3 *Presence of the host cell*

As discussed earlier, the presence of the host cell imposes a constraint on the height of the viral membrane deformation and we examine this effect in Fig. 9. In Fig. 9(a), the shape of the viral membrane

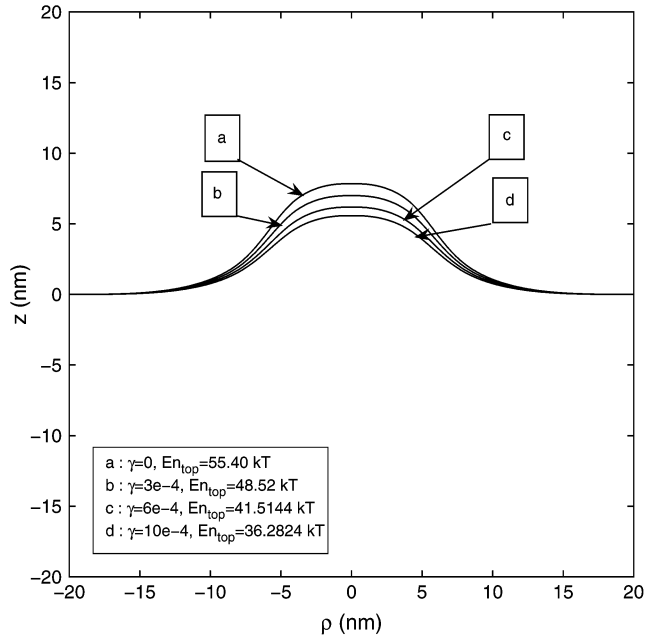

FIG. 8. Deformation affected by membrane tension: larger tension leads to less deformation.

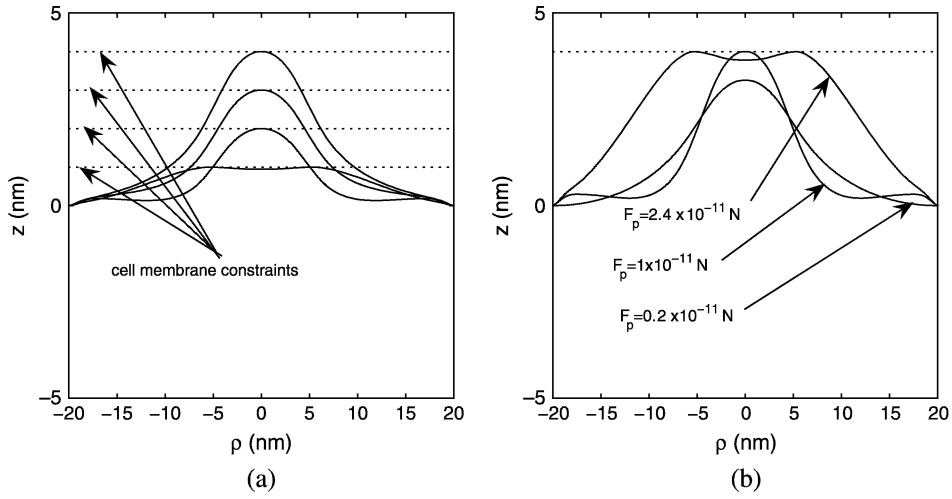

FIG. 9. (a) Deformation of the viral membrane constrained by different heights under same bending moments. (b) Deformation of the viral membrane under different bending moments exerted by the protein with a fixed maximum height constraint.

is obtained by setting the maximum height at 4, 3, 2 and 1 nm while other conditions are kept the same. It can be seen that due to the height constraint, the dimple top becomes flat. In Fig. 9(b), we vary the bending moments exerted by protein while fixing the maximum height. The viral membrane shape begins to flatten and even form a 'reversed dimple' (with negative curvatures) as the bending moments

due to the protein cluster increase. More detail understanding of the interaction and coupling between viral and host cell membranes can be gained by extending our model which will be pursued in the future.

5. Conclusion

We have presented a mathematical model for the pre-fusion process of viral infection mediated by HA protein. The deformation of the viral membrane and energy stored in the membrane are computed using the Euler–Lagrange equations based on a Helfrich-type energy functional.

Our results on dimple formation due to the asymmetric nature of protein molecules confirm a hypothesis in the literature that pre-fusion deformation can be mediated by HA protein clusters. The energy stored in the dimple top predicted by our model is at a physically reasonable level to facilitate merging of the contacting bilayers. Our results show that there exists an optimal fusion-site size and a spontaneous curvature corresponding to a maximum dimple height and energy stored inside the dimple top. Dimple height and energy stored inside the dimple top are positively correlated with protein cluster size and bending moments (i.e. the moments' difference in two principal directions) exerted by the protein. Furthermore, membrane tension plays a role in the membrane shape as well as energy stored inside the dimple top. Membranes with tension resist bending and therefore reduce the chance for contact and fusion. Spontaneous curvature can either favour or inhibit fusion. The predictions based on our model are consistent with experimental observations in the literature. The shape of the viral membrane constrained by the presence of a cell membrane depends upon the location of the cell membrane as well as the magnitude of the bending moment exerted by the protein.

Finally, we note that for studying dimple formation during the pre-fusion stage, it is sufficient to treat the bilayer as a single membrane without distinguishing the two monolayers. As a consequence of the dimple formation, the viral and host membranes come into close contact which eventually leads to membrane fusion. It is believed that fusion starts with the merge of two contacting monolayers in a step by step fashion. In order to model the fusion process in more detail, we plan to generalize our model by considering individual monolayers instead of bilayers. This can be achieved by generalizing the Helfrich energy functional.

Acknowledgements

Part of the research is supported by the Natural Science and Engineering Research Council of Canada. One of the authors (H.H.) wishes to thank Japan Society for the Promotion of Sciences for providing a visiting fellowship while part of this research was carried out. Authors would also like to thank the referees and Dr Sean Bohun for their valuable comments.

References

BENTZ, J. (2000) Membrane fusion mediated by coiled coils: a hypothesis. *Biophys. J.*, **78**, 886–900.

BENTZ, J., ELLENS, H. & ALFORD, D. (1990) An architecture for the fusion site of influenza hemagglutinin. *FEBS Lett.*, **276**, 1–5.

BLUMENTHAL, R., CLAGUE, M. J., DURELL, S. R. & EPAND, R. M. (2003) Membrane fusion. *Chem. Rev.*, **103**, 53–69.

BLUMENTHAL, R., PAK, C. C., RAVIV, Y., KRUMBIEGEL, M., BERGELSON, L. D., MORRIS, S. J. & LOWY, R. J. (1995) Transient domains induced by influenza hemagglutinin during membrane fusion. *Mol. Membr. Biol.*, **12**, 135–142.

BLYTH, M. G. & POZRIKIDIS, C. (2004) Solution space of axisymmetric capsules enclosed by elastic membranes. *Eur. J. Mech. A/Solids*, **23**, 877–892.

BOAL, D. (2002) *Mechanics of the Cell*. Cambridge, UK: Cambridge University Press.

BULLOUGH, P. A., HUGHSON, F. M., SKEHEL, J. J. & WILEY, D. C. (1994) Structure of influenza hemagglutinin at the pH of membrane fusion. *Nature*, **371**, 37–43.

CARR, C. M. & KIM, P. S. (1993) A spring-loaded mechanism for the conformational change of influenza hemagglutinin. *Cell*, **73**, 823–832.

DANIELI, T., PELLETIER, S. L., HENIS, Y. I. & WHITE, J. M. (1996) Membrane fusion mediated by the influenza virus hemagglutinin requires the concerted action of at least three hemagglutinin trimers. *J. Cell Biol.*, **133**, 559–569.

DERGANC, J., BOZIC, B., SVETINA, S. & ZEKS, B. (2003) Equilibrium shape of erythrocytes in rouleau formation. *Biophys. J.*, **84**, 1486–1492.

GAUDIN, Y., RUIGROK, R. W. H. & BRUNNER, J. (1995) Low-pH induced conformational changes in viral fusion proteins: implications for the fusion mechanism. *J. Gen. Virol.*, **76**, 1541–1556.

GERE, J. M. (2004) *Mechanics of Materials*. Belmont, CA: Brooks/Cole, Thomson.

GRUENKE, J. A., ARMSTRONG, R. T., NEWCOMB, W. W., BROWN, J. C. & WHITE, J. M. (2002) New insights into the spring-loaded conformational change of influenza virus hemagglutinin. *J. Virol.*, **76**, 4456–4466.

GUTMAN, O., DANIELI, T., WHITE, J. M. & HENIS, Y. I. (1993) Effects of exposure to low pH on the lateral mobility of influenza hemagglutinin expressed at the cell surface: correlation between mobility inhibition and inactivation. *Biochemistry*, **32**, 101–106.

HELFRICH, W. (1973) Elastic properties of lipid bilayers-theory and possible experiments. *Z. Naturforsch*, **28c**, 693.

HIBBELER, R. C. (2005) *Mechanics of Materials*. Upper Saddle River, NJ: Pearson Prentice Hall.

HU, J.-G. & OU-YANG, Z.-C. (1993) Shape equations of the axisymmetric vesicles. *Phys. Rev. E*, **47**, 461–467.

JULICHER, F. & LIPOWSKY, R. (1996) Shape transformations of vesicles with intra-membrane domains. *Phys. Rev. E*, **53**, 2670–2683.

JULICHER, F. & SEIFERT, U. (1994) Shape equations for axisymmetric vesicles: a clarification. *Phys. Rev. E*, **49**, 4728–4731.

KOZLOV, M. M. & CHERNOMORDIK, L. V. (1998) A mechanism of protein-mediated fusion: coupling between refolding of the influenza hemagglutinin and lipid rearrangements. *Biophys. J.*, **75**, 1384–1396.

KOZLOV, M. M. & CHERNOMORDIK, L. V. (2002) The protein coat in membrane fusion: lessons from fission. *Traffic Interchange*, **3**, 256–267.

KOZLOVSKY, Y., CHERNOMORDIK, L. V. & KOZLOV, M. M. (2002) Lipid intermediates in membrane fusion: formation, structure and decay of hemifusion diaphragm. *Biophys. J.*, **83**, 2634–2651.

KOZLOVSKY, Y. & KOZLOV, M. M. (2002) Stalk model of membrane fusion: solution of energy crisis. *Biophys. J.*, **82**, 882–895.

KUZMIN, P. I., ZIMMERBERG, J., CHIZMADZHEV, Y. A. & COHEN, F. S. (2001) A quantitative model for membrane fusion based on low-energy intermediates. *Proc. Natl. Acad. Sci.*, **98**, 7235–7240.

LI, Y., HAN, X., LAI, A. L., BUSHWELLER, J. H., CAFISO, D. S. & TAMM, L. K. (2005) Membrane structures of the hemifusion-inducing fusion peptide mutant G1S and the fusion-blocking mutant G1V of influenza virus hemagglutinin suggest a mechanism for pore opening in membrane fusion. *J. Virol.*, **79**, 12065–12076.

MARKIN, V. S. & ALBANESI, J. P. (2002) Membrane fusion: Stalk model revisited. *Biophys. J.*, **82**, 693–712.

MARKOSYAN, R. M., MELIKYAN, G. B. & COHEN, F. S. (1999) Tension of membranes expressing the Hemagglutinin of influenza virus inhibits fusion. *Biophys. J.*, **77**, 943–952.

MARKOVIC, I., LEIKINA, E., ZHUKOVSKY, M., ZIMMERBERG, J. & CHERNOMORDIK, L. V. (2001) Synchronized activation and refolding of influenza hemagglutinin in multimeric fusion machines. *J. Cell Biol.*, **155**, 833–843.

MAY, S. (2002) Structure and energy of fusion stalks: the role of membrane edges. *Biophys. J.*, **83**, 2969–2980.

NAITO, H., OKUDA, M. & OU-YANG, Z.-C. (1993) Counterexample to some shape equations for axisymmetric vesicles. *Phys. Rev. E*, **48**, 2304–2307.

OU-YANG, Z.-C. & HELFRICH, W. (1989) Bending energy of vesicle membranes: general expressions for the first, second and third variation of the shape energy and applications to spheres and cylinders. *Phys. Rev. A*, **39**, 5280–5288.

POZRIKIDIS, C. (2003) Shell theory for capsules and cells. *Modeling and Simulation of Capsules and Biological Cells* (C. Pozrikidis ed.). Boca Raton, FL: (C. Pozrikidis ed.) Chapman & Hal, pp. 35–101.

POZRIKIDIS, C. (2005) Resting shape and spontaneous membrane curvature of red blood cells. *Math. Med. Biol.*, **22**, 34–52.

SAGE, A. P. (1968) *Optimal Systems Control*. Englewood Cliffs, NJ: Prentice-Hall.

SEIFERT, U. (1997) Configurations of fluid membranes and vesicles. *Adv. Phys.*, **46**, 13–137.

SKEHEL, J. J. & WILEY, D. C. (2000) Receptor binding and membrane fusion in virus entry: the influenza hemagglutinin. *Annu. Rev. Biochem.*, **69**, 531–569.

STEGMANN, T. (1993) Influenza hemagglutinin-mediated membrane fusion does not involve inverted phase lipid intermediates. *J. Biol. Chem.*, **268**, 1716–1722.

TAMM, L. K. (2003) Hypothesis: spring-loaded boomerang mechanism of influenza hemagglutinin-mediated membrane fusion. *Biochem. Biophys. Acta*, **1614**, 14–23.

TAMM, L. K., ABILDGAARD, F., ARORA, A., BLAD, H. & BUSHWELLER, J. H. (2003a) Structure, dynamics and function of the outer membrane protein A (OmpA) and influenza hemagglutinin fusion domain in detergent micelles by solution NMR. *FEBS Lett.*, **555**, 139–143.

TAMM, L. K., CRANE, J. & KIESSLING, V. (2003b) Membrane fusion: a structural perspective on the interplay of lipids and proteins. *Curr. Opin. Struct. Biol.*, **13**, 453–466.

TATULIAN, S. A., HINTERDORFER, P., BABER, G. & TAMM, L. K. (1995) Influenza hemagglutinin assumes a tilted conformation during membrane fusion as determined by attenuated total reflection FTIR spectroscopy. *EMBO J.*, **14**, 5514–5523.

VAIDYA, N., HUANG, H. & TAKAGI, S. (2006) Correct equilibrium shape equation of axisymmetric vesicles. *Proceedings of Ninth International Conference of Integral Methods in Science and Engineering, Niagara Falls, Canada, July 23–27, 2006*. Available at http://www.math.yorku.ca/ ∼nvaidya/IMSEpaper.pdf.

WILEY, D. C. & SKEHEL, J. J. (1987) The structure and function of the hemagglutinin membrane glycoprotein of influenza virus. *Annu. Rev. Biochem.*, **56**, 365–394.

ZHENG, W. & LIU, J. (1993) Helfrich shape equation for axisymmetric vesicles as a first integral. *Phys. Rev. E*, **48**, 2856–2860.

ZIMMERBERG, J., VOGEL, S. S. & CHERNOMORDIK, L. V. (1993) Mechanism of membrane fusion. *Annu. Rev. Biophys. Biomol. Struct.*, **22**, 433–466.

Appendix A. Derivation of axisymmetric shape equations

There are a number of ways to derive the axisymmetric shape equation. Obviously, one can try to derive the general shape equation in 3D by modifying the approach in Ou-Yang & Helfrich (1989) and apply the condition of axisymmetry. A more appealing alternative is to work with the axisymmetric form of the energy functional before applying the calculus of variations. However, there have been some concerns and confusion related to this approach (Blyth & Pozrikidis, 2004; Hu & Ou-Yang, 1993; Naito *et al.*, 1993; Pozrikidis, 2003; Seifert, 1997) and it has been argued in Hu & Ou-Yang (1993) that the variation has to be performed in the normal direction to obtain the correct shape equation. In Julicher & Seifert

(1994), it was shown that the same equation of axisymmetric vesicles (closed lipid bilayer membranes) can be obtained by both approaches. The main conclusion was that an additional equation needs to be introduced for the Hamiltonian (i.e. constant Hamiltonian) with a proper treatment of the boundary conditions. However, the treatment of boundary conditions is not straightforward for fixed integral limits (constant total arc length) and the validity of the argument was again questioned recently (Blyth & Pozrikidis, 2004; Pozrikidis, 2003). Moreover, most of the derivations used the energy functional with the arc length s as a primary variable, while in some cases it maybe advantageous to use the distance from the axis of symmetry ρ as a primary variable. As pointed out in Hu & Ou-Yang (1993), derivation of the Euler–Lagrange equation corresponding to the energy functional with ρ as a primary variable might produce an erroneous equation.

In this appendix, we explicitly state the conditions for obtaining shape equations related to the energy functional (2.1), with ρ as a primary variable. The derivation related to (2.2) is similar and is omitted. Vaidya *et al.* (2006) have shown that the variation in the direction perpendicular to the axis of symmetry can also produce the correct shape equation if the induced variation in other variables is obtained by using a proper geometric constraint. Therefore, the variation does not have to be in the normal direction. We further demonstrate that to obtain the correct shape equation of the axisymmetric membrane, we only need to impose an equivalent condition $\cos\psi\,\mathrm{d}z + \sin\psi\,\mathrm{d}\rho = 0$ while performing the variation. We note that our approach is not restricted to the pre-fusion deformation of a membrane segment and can be applied to vesicle shape as well (Vaidya *et al.*, 2006). Finally, it is worth noting that similar geometric conditions are suggested by Julicher & Seifert (1994) for vesicles. However, these conditions have not been implemented in their later work (Derganc *et al.*, 2003; Julicher & Lipowsky, 1996).

Under axisymmetric conditions, we have $c_1 = \cos\psi(\mathrm{d}\psi/\mathrm{d}\rho)$ and $c_2 = \sin\psi/\rho$. We incorporate the geometric condition $\cos\psi(\mathrm{d}z/\mathrm{d}\rho) + \sin\psi = 0$ in the energy functional (2.1) via an additional Lagrange multiplier η as follows:

$$\hat{E}_1 = \pi \int_0^{\rho_f} \left[\frac{k_\mathrm{b}\rho}{\cos\psi}\left(\cos\psi\frac{\mathrm{d}\psi}{\mathrm{d}\rho} + \frac{\sin\psi}{\rho} - c_0\right)^2 + \frac{\rho}{\cos\psi}\left(f_\mathrm{p}^{(1)}\cos\psi\frac{\mathrm{d}\psi}{\mathrm{d}\rho} + f_\mathrm{p}^{(2)}\frac{\sin\psi}{\rho}\right) \right.$$
$$\left. + \eta\left(\cos\psi\frac{\mathrm{d}z}{\mathrm{d}\rho} + \sin\psi\right)\right]\mathrm{d}\rho. \tag{A.1}$$

Taking the first variation and using product rule, we get

$$\delta\hat{E}_1 = \pi \int_0^{\rho_f} \left[\frac{2k_\mathrm{b}\rho}{\cos\psi}\left(\cos\psi\frac{\mathrm{d}\psi}{\mathrm{d}\rho} + \frac{\sin\psi}{\rho} - c_0\right)\left\{\cos\psi\,\delta\left(\frac{\mathrm{d}\psi}{\mathrm{d}\rho}\right) - \sin\psi\frac{\mathrm{d}\psi}{\mathrm{d}\rho}\delta\psi + \frac{\cos\psi}{\rho}\delta\psi\right\}\right.$$
$$+ \frac{k_\mathrm{b}\rho\sin\psi}{\cos^2\psi}\left(\cos\psi\frac{\mathrm{d}\psi}{\mathrm{d}\rho} + \frac{\sin\psi}{\rho} - c_0\right)^2\delta\psi + f_\mathrm{p}^{(1)}\rho\delta\left(\frac{\mathrm{d}\psi}{\mathrm{d}\rho}\right) + \frac{f_\mathrm{p}^{(2)}}{\cos^2\psi}\delta\psi$$
$$\left. + \left(\cos\psi\frac{\mathrm{d}z}{\mathrm{d}\rho} + \sin\psi\right)\delta\eta + \eta\left\{\cos\psi\,\delta\left(\frac{\mathrm{d}z}{\mathrm{d}\rho}\right) - \sin\psi\frac{\mathrm{d}z}{\mathrm{d}\rho}\delta\psi + \cos\psi\,\delta\psi\right\}\right]\mathrm{d}\rho. \tag{A.2}$$

Performing an integration by parts and simplifying, we obtain

$$\begin{aligned}\delta\hat{E}_1 = \pi \int_0^{\rho_f} \Bigg[& k_b \rho \sin\psi \left(\frac{d\psi}{d\rho}\right)^2 + \frac{k_b \sin\psi}{\rho} + \frac{k_b \sin\psi}{\rho \cos^2\psi} - 2k_b \rho \cos\psi \frac{d^2\psi}{d\rho^2} - 2k_b \cos\psi \frac{d\psi}{d\rho} \\ & - f_p^{(1)} - \rho \frac{d f_p^{(1)}}{d\rho} + \frac{f_p^{(2)}}{\cos^2\psi} + \frac{k_b c_0^2 \rho \sin\psi}{\cos^2\psi} - \frac{2k_b c_0 \sin^2\psi}{\cos^2\psi} + \frac{\eta}{\cos\psi} \Bigg] \delta\psi \, d\rho \\ & + \pi \int_0^{\rho_f} \left[\cos\psi \frac{dz}{d\rho} + \sin\psi \right] \delta\eta \, d\rho + \pi \int_0^{\rho_f} \left[\eta \sin\psi \frac{d\psi}{d\rho} - \cos\psi \frac{d\eta}{d\rho} \right] \delta z \, d\rho \\ & + \pi \left[\left(2k_b \rho \cos\psi \frac{d\psi}{d\rho} + 2k_b \sin\psi + f_p^{(1)} \rho - 2k_b c_0 \rho \right) \delta\psi \right] \Bigg|_0^{\rho_f} \\ & + \pi \left[(\eta \cos\psi) \, \delta z \right]_0^{\rho_f} . \end{aligned} \tag{A.3}$$

Using the boundary conditions $\psi(0) = \psi(\rho_f) = 0$ (Section 3.4), the second to last term of (A.3) vanishes. Since at the boundary $\rho = 0$, the variable z has to satisfy the condition $dz/d\rho = -\tan\psi = 0$, we are not allowed an arbitrary variation δz at $\rho = 0$. Therefore, using $\delta z|_{\rho=0} = 0$ and the boundary condition $z|_{\rho=\rho_f} = z_f$ given in Section 3.4, the last term of (A.3) vanishes. Since the variations $\delta\psi$, $\delta\eta$ and δz are arbitrary, we obtain the necessary conditions for a minimum energy by forcing the coefficients of $\delta\psi$, $\delta\eta$ and δz to vanish, which leads to the following Euler–Lagrange equations:

$$\begin{aligned} & k_b \rho \sin\psi \left(\frac{d\psi}{d\rho}\right)^2 + \frac{k_b \sin\psi}{\rho} + \frac{k_b \sin\psi}{\rho \cos^2\psi} - 2k_b \rho \cos\psi \frac{d^2\psi}{d\rho^2} - 2k_b \cos\psi \frac{d\psi}{d\rho} \\ & \quad - f_p^{(1)} - \rho \frac{d f_p^{(1)}}{d\rho} + \frac{f_p^{(2)}}{\cos^2\psi} + \frac{k_b c_0^2 \rho \sin\psi}{\cos^2\psi} - \frac{2k_b c_0 \sin^2\psi}{\cos^2\psi} + \frac{\eta}{\cos\psi} = 0, \qquad \text{(A.4a)} \\ & \cos\psi \frac{dz}{d\rho} + \sin\psi = 0, \qquad \text{(A.4b)} \\ & \eta \sin\psi \frac{d\psi}{d\rho} - \cos\psi \frac{d\eta}{d\rho} = 0. \qquad \text{(A.4c)} \end{aligned}$$

After simplification, (A.4a)–(A.4c) become (3.3a)–(3.3c).

REMARK We note that the equations derived here correspond to the correct shape equations obtained in the literature (Blyth & Pozrikidis, 2004; Hu & Ou-Yang, 1993; Julicher & Seifert, 1994; Naito *et al.*, 1993; Pozrikidis, 2003; Zheng & Liu, 1993), by setting $f_p^{(1)} = f_p^{(2)} = 0$. To see this, we rewrite (A.4a) as $\eta = \eta\left(\rho, \psi, d\psi/d\rho, d^2\psi/d\rho^2\right)$, compute $d\eta/d\rho$ and substitute both into (A.4c). A more direct comparison on vesicle shape equations can be found in Vaidya *et al.* (2006).

Appendix B. Solution methodology

In this section, we briefly explain how to solve the Euler–Lagrange equations derived earlier. We use the system (3.3a)–(3.3c) as an example as the method for the systems (3.5a)–(3.5c) and (3.9a), (3.9b), (3.9e), (3.9f) are similar. To solve the system of ordinary differential equations (3.3a)–(3.3c) with boundary conditions (3.7a) and (3.7b), we use the finite-difference method. At the boundaries in which Neumann's

boundary conditions are given, we determine numerically the boundary values by using a Taylor expansion with the given boundary conditions. We use the following numerical scheme to solve system (3.3a)–(3.3c).

Let $\Delta\rho = \rho_f/(N+1)$ be the grid size so that $\rho_i = i\,\Delta\rho$, $i = 0, 1, 2, \ldots, (N+1)$, forms a partition of $[0, \rho_f]$. We assume that ψ_i and z_i are approximations to ψ and z, respectively, at the grid point ρ_i, $i = 1, 2, \ldots, N$. On this uniform grid, we use the following discretization schemes:

$$\left.\frac{\mathrm{d}^2\psi}{\mathrm{d}\rho^2}\right|_{\rho_i} = \frac{\psi_{i+1} - 2\psi_i + \psi_{i-1}}{(\Delta\rho)^2}, \tag{B.1a}$$

$$\left.\frac{\mathrm{d}\psi}{\mathrm{d}\rho}\right|_{\rho_i} = \frac{\psi_{i+1} - \psi_{i-1}}{2\Delta\rho}, \tag{B.1b}$$

$$\left.\frac{\mathrm{d}z}{\mathrm{d}\rho}\right|_{\rho_i} = \frac{z_{i+1} - z_i}{\Delta\rho}. \tag{B.1c}$$

After substituting η from (3.3c) in (3.3a), the system (3.3a)–(3.3b) can be discretized as

$$\begin{aligned}
&\cos^2\psi_i\left[\frac{\psi_{i+1} - 2\psi_i + \psi_{i-1}}{(\Delta\rho)^2}\right] - \frac{\sin 2\psi_i}{4}\left[\frac{\psi_{i+1} - \psi_{i-1}}{\Delta\rho}\right]^2 \\
&- \frac{\sin 2\psi_i}{4\rho_i^2} - \frac{\sin\psi_i}{2\rho_i^2\cos\psi_i} + \frac{\cos^2\psi_i}{\rho_i}\left[\frac{\psi_{i+1} - \psi_{i-1}}{2\Delta\rho}\right] + \frac{f_{\mathrm{p}}^{(1)}(\rho_i)\cos\psi_i}{2k_{\mathrm{b}}\rho_i} \\
&+ \frac{\cos\psi_i}{2k_{\mathrm{b}}}\left.\frac{\mathrm{d}\,f_{\mathrm{p}}^{(1)}}{\mathrm{d}\rho}\right|_{\rho_i} - \frac{f_{\mathrm{p}}^{(2)}(\rho_i)}{2k_{\mathrm{b}}\rho_i\cos\psi_i} - \frac{\eta_0}{2k_{\mathrm{b}}\rho_i\cos\psi_i} - \frac{c_0^2\sin\psi_i}{2\cos\psi_i} + \frac{c_0\sin^2\psi_i}{\rho_i\cos\psi_i} = 0,
\end{aligned} \tag{B.2a}$$

$$\cos\psi_i\frac{z_{i+1} - z_i}{\Delta\rho} + \sin\psi_i = 0, \tag{B.2b}$$

$$i = 1, 2, \ldots, N.$$

Using boundary conditions (3.7a) and (3.7b), this scheme produces a system of $2N-1$ nonlinear equations with $2N-1$ unknowns $\psi_1, \psi_2, \ldots, \psi_{N-1}, z_1, z_2, \ldots, z_{N-1}, \eta_0$. Using similar procedures, we obtain $2N-1$ equations with $2N-1$ variables by discretizing (3.5a)–(3.5c) and $4N$ equations with $4N$ variables by discretizing (3.9a), (3.9b), (3.9e), (3.9f). The resulting system of nonlinear algebraic equations are solved by using 'fsolve.m' in the optimization toolbox of MATLAB, which implements the Gauss–Newton method with line search. The Gauss–Newton method uses a nonlinear least-squares solver which employs a line-search procedure and a quasi-Newton method to solve the equations. On varying N from 500 to 2000, we obtained the same result. Therefore, the results presented here are for $N = 500$. In our simulation, optimization was terminated when the magnitude of search direction is less than 10^{-8} and the residual is less than 4.89×10^{-20}. The run time for each case varies between 5 and 20 min on a Pentium IV Dell laptop.